doi:10.1093/jmcb/mju044
Published online November 17, 2014



# Article

# Molecular dynamics reveal a novel kinase–substrate interface that regulates protein translation

Ming S. Liu[1,2,†,*], Die Wang[1,†], Hiroyuki Morimoto[1,3], Howard C.H. Yim[1], Aaron T. Irving[1], Bryan R.G. Williams[1,4], and Anthony J. Sadler[1,4,*]

[1] Centre for Cancer Research, MIMR-PHI Institute of Medical Research, Melbourne, VIC 3168, Australia
[2] CSIRO – Computational Informatics and Digital Productivity Flagship, Private Bag 10, Clayton South, VIC 3169, Australia
[3] Department of Anatomy, School of Medicine, University of Occupational and Environmental Health, Kitakyushu, Fukuoka 807-8555, Japan
[4] Department of Molecular and Translational Science, Monash University, Melbourne, VIC 3168, Australia
[†] These authors contributed equally to this work.
[*] Correspondence to: Anthony J. Sadler, E-mail: anthony.sadler@mimr-phi.org; Ming S. Liu, E-mail: ming.liu@csiro.au

**A key control point in gene expression is the initiation of protein translation, with a universal stress response being constituted by inhibitory phosphorylation of the eukaryotic initiation factor 2α (eIF2α). In humans, four kinases sense diverse physiological stresses to regulate eIF2α to control cell differentiation, adaptation, and survival. Here we develop a computational molecular model of eIF2α and one of its kinases, the protein kinase R, to simulate the dynamics of their interaction. Predictions generated by coarse-grained dynamics simulations suggest a novel mode of action. Experimentation substantiates these predictions, identifying a previously unrecognized interface in the protein complex, which is constituted by dynamic residues in both eIF2α and its kinases that are crucial to regulate protein translation. These findings call for a reinterpretation of the current mechanism of action of the eIF2α kinases and demonstrate the value of conducting computational analysis to evaluate protein function.**

**Keywords:** molecular dynamics, eukaryotic initiation factor 2α (eIF2α), eIF2α kinases, protein kinase R (PKR), protein translation, kinase activity

## Introduction

Adaptive responses to changing environmental conditions require switching between various genetic programs. Gene expression is regulated at multiple steps including transcription, posttranscriptional processing, nuclear export, stability and translation of mature mRNA. A key control point in gene expression is the initiation of protein translation. Translation of eukaryotic transcripts generally commences through an association between the 5′ cap structure of mRNA and the 43S pre-initiation complex, consisting of eukaryotic initiation factors (eIF) 1, 3 and 4 and the ternary complex, formed between eIF2α, guanine-5′-triphosphate (GTP), and the initiator Met-tRNA. This pre-initiation complex then scans the mRNA toward the 3′ end until the Met-tRNA anticodon matches a functional AUG codon, GTP is hydrolysed, and the eIF2α-GDP is released from the complex, whereupon the 60S ribosomal subunit is recruited to assemble the functional ribosome. This initiation step constitutes a pivotal point for regulation of gene expression in eukaryotes, with a key means of control enacted by phosphorylation of eIF2α. Phosphorylation of eIF2α, at the serine residue number 51, increases the affinity of the guanine nucleotide exchange factor eIF2B. This association prevents exchange of GDP as is required for reformation of the ternary complex to allow translation re-initiation.

In mammals, four serine, threonine kinases respond to different physiological stresses to phosphorylate eIF2α (Sadler and Williams, 2007). These are the heme-regulated inhibitor (HRI), RNA-activated protein kinase R (PKR), PKR-like endoplasmic reticulum (PERK), and general control nonderepressing 2-like (GCN2) kinases (encoded by the genes *EIF2AK1* to *4*, respectively). Crystallographic structures of the modified kinase domains of GCN2 and PERK alone, and the PKR kinase domain associated with eIF2α have been resolved (Dar et al., 2005; Padyana et al., 2005; Cui et al., 2011). The structure of PKR bound to eIF2α is highly informative to our understanding of the molecular mechanism of activity of the eIF2α kinases.

PKR consists of an N-terminal RNA-binding domain (RBD), encoding tandem RNA-binding motifs and a C-terminal kinase domain (KD), which forms an archetypal kinase fold consisting of an N-lobe that coordinates dimerization of protein monomers and a C-lobe that mediates substrate associations. Unstructured linkers separate each of these structured domains. Ligand binding triggers dimerization and concurrent autophosphorylation to form the

Received March 31, 2014. Revised August 28, 2014. Accepted September 10, 2014.

active enzyme. Structure studies identified how PKR phosphorylated the critical serine 51 residue of eIF2α. This serine residue is within a linker between β3-β4 in eIF2α that is buried in a hydrophobic pocket. The crystal structure identified that residues within the helix G (αG) in the C-lobe of the KD bound eIF2α to correctly orient eIF2α toward the catalytic cleft of the KD. Binding at the αG of PKR unfolded the β3-β4 loop of eIF2α in a manner that was speculated, as the serine 51 linker was unresolved in crystallographic structures, to expose the phosphor-residue.

As the peptides used to deduce all crystallographic structures of the eIF2α kinases contain large internal deletions of key interfacing segments and because current structures do not capture a critical component of enzymatic activity, the dynamic movement of the proteins, we developed a molecular model of the complete kinase domain of PKR and eIF2α to tackle the dynamics of their interaction by coarse-grained dynamics simulation. This predicts that residues within the kinase N-lobe, which were removed from peptides used to generate crystallographic structures, and the unresolved serine 51 linker in eIF2α are engaged in the contact between the molecules. Experimentation corroborates this by demonstrating that these dynamic residues in PKR are crucial for effective control of eIF2α activity and protein translation. These findings identify a novel mode of action of the eIF2α kinases.

## Results

### *Molecular dynamic modeling of eIF2α*

A complete N-terminal peptide structure of the human eIF2α molecule was generated using the partial PKR–eIF2α complex and a structure of the *Saccharomyces cerevisiae* eIF2α (SUI2) (using PDB:2A1A and PDB:1Q46, respectively). The original unresolved loop of eIF2α (between residues 49 and 60) was modeled in two states, coded 'open' and 'closed', which represented the preferred, energy-minimized states predicted by molecular dynamics from an ensemble of all possible orientations (Figure 1A). The 'closed' state of the residues within the β3-β4 loop, was constructed by superposition, firstly, on the crystal structure of eIF2α, then on the eIF2α-PKR complex (where the residues 49–60 are missing). Dynamics modeling to randomly sample the β3-β4 loop identified an energetically favored conformational state in which the constrained state of this region, seen in the crystal structure, had moved to an opposite more open position. This 'open' state was then constructed by superposition onto the eIF2α-PKR complex. Both orientations, coded 'open' and 'closed', were modeled in the subsequent analysis.

Comparison of the theoretical and experimentally derived states of eIF2α shows general agreement, except for a conspicuous variance in the flexibility of the restored residues (49–60), when this loop was modeled in the open state (Figure 1B). This is likely significant as these residues encompass the phosphorylated residue (Ser51) that is critical for enzymatic activity. Ile55-Ile58 at the tip of the loop is constrained in the closed state, but unconfined in the open state. Intriguingly, residues between Arg74-Asp83 are highly dynamic in both theoretical states, but are constrained in the crystal structure (Figure 1B). These residues have previously been identified to contact PKR within the kinase helix αG (Dar et al., 2005). This modeling predicts that the previously unresolved region encompassing the phosphor-residue adopts quite distinct states.

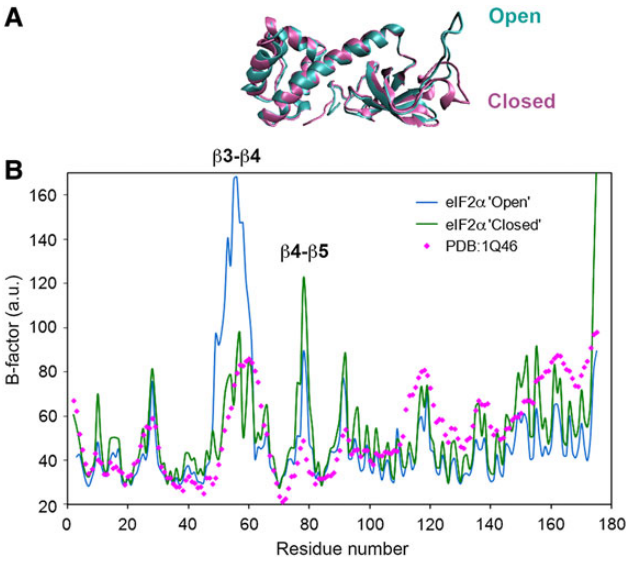


**Figure 1** Dynamics of alternate states of eIF2α. (**A**) The complete structures shown as a ribbon diagram of the N-terminus of human eIF2α in two predicted conformations, designated as open (colored cyan), or closed (purple), as defined by the orientation of the β3-β4 loop (residues 49–60) absent from PDB:2A1A. (**B**) Fluctuation and flexibility differences (as indicated by B-factor) between the open (blue line) and closed (green line) theoretical conformational states compared with the values calculated from the experimentally derived (pink diamonds) structure of eIF2α.

### *Modeling of the association of eIF2α with PKR*

In order to probe eIF2α-PKR interactions, we first generated a full-length theoretical structure of PKR by correcting mutated and missing residues from the high-resolution structures of the RBD of PKR and the KD in complex with eIF2α (using RCSB files PDB:1QU6 and PDB:2A1A, respectively). Homology modeling and dynamics simulation of the linker between the RBD and KD (residues 175–254) corroborated previous studies that have shown this linker to be unstructured and to have high dynamic flexibility (VanOudenhove et al., 2009). For this reason and to be able to directly compare our theoretical structures to existing experimental data, we excluded the RBD and linker from the simulations of the interaction with eIF2α. This was used to model the structure of the dimerized kinase in association with eIF2α in either of the predicted open and closed states (Figure 2A and B), and compared with the experimentally derived structure of the dimerized KD-eIF2α complex.

This analysis predicts that residues within the β1-β2 (Gly276-Gly277), β4-β5 (Glu349-Ser351), αE (Lys388-Leu390), p+1 loop (centered upon Thr451), and helix αG (Val484-Glu490) structural elements of PKR were most affected by substrate binding, with differing consequence for either theoretical state of eIF2α (Figure 2C and D). Four of these elements have previously been established

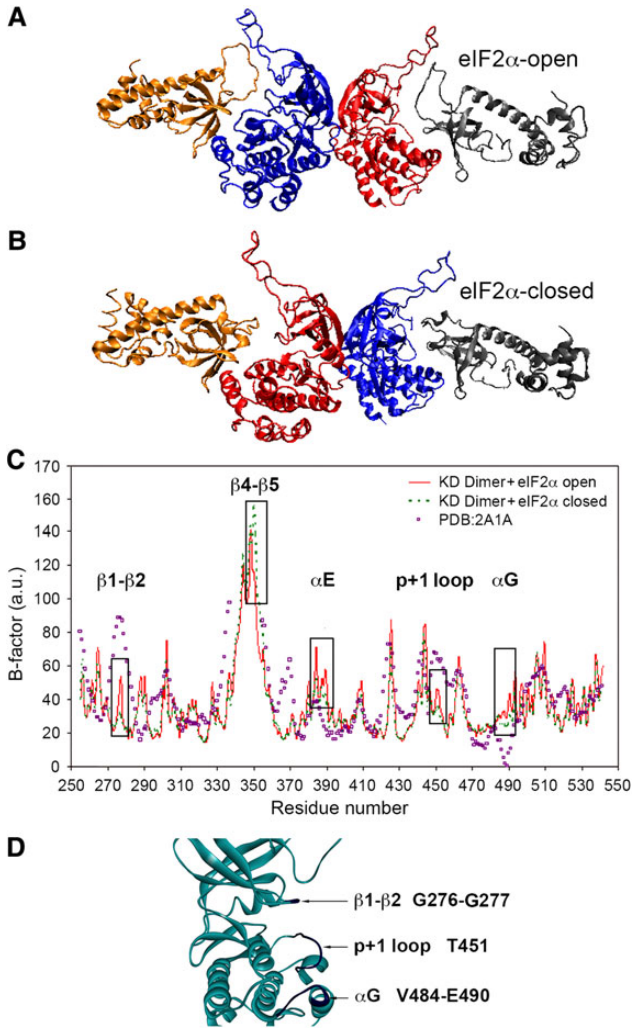


**Figure 2** Dynamic impacts due to the interaction of PKR with eIF2α. (**A** and **B**) Theoretical structures shown as ribbon diagrams of the dimeric KD (with each protomer colored blue and red) in complex with eIF2α (colored gray and yellow) in either an open (**A**), or closed (**B**) conformation. The structures demonstrate the proximity between the restored β4-β5 loop in the N-lobe of PKR and the β3-β4 loop in eIF2α when in the open conformation. The β4-β5 loop of PKR is flexible and molecular dynamics did not give any clearly defined conformation after extended dynamics equilibration. Moreover, a conformation could not be assigned by reference to the crystal structure of the eIF2α–PKR complex (as the residues 338–350 are missing), so the state of the β4-β5 loop shown in this figure is the average conformation ensemble from coarse-grained simulations. (**C**) Fluctuation and flexibility differences (as indicated by B-factor) for the theoretical KD dimer associated with eIF2α in either the open (solid red line), or closed (broken green line) conformation, compared with the experimentally derived KD-eIF2α complex (purple squares). The boxed areas indicate PKR residues predicted to be differentially affected by the alternate conformations of eIF2α (open or closed). (**D**) A ribbon diagram of the structure of the catalytic pocket of PKR indicating (in dark blue) the residues encompassing the β1-β2 loop (Gly276 and Gly277), autophosphorylated Thr451 in the activation segment and part of αG (Val484-Glu490) predicted to be highly dynamic during substrate binding.

to interact with eIF2α, or ATP to facilitate phosphoryl transfer (Dar and Sicheri, 2002). These residues encode the kinase glycine-rich loop (Gly276-Gly277), an essential autophosphorylation site (Thr451), part of the kinase activation segment (Lys388-Leu390) and the eIF2α-binding consensus motif (Val484-Glu490), which are required for PKR activity. However, the β4-β5 loop in the N-lobe has no reported contact with eIF2α and no recognized catalytic activity.

Residues coincident with and separate from these five regions differed between the theoretical and experimentally derived data. Residues within the β1-β2 and p+1 loop showed greater, while those in the helical αE and αG elements showed less constraint in the experimental compared with the theoretical data. There were also discrepancies outside of these five regions, with B-factors predicting altered constraint for residues within the αO, β2, αC and αF, β3, β4, β5-αD, β9, and αH elements for the experimental compared with the theoretical data. As the β4-β5 loop was removed from the peptide used to generate the experimental data, this comparison cannot be made.

Together, these findings indicate that dynamic residues on the N-lobe of the kinase domain, between β4 and β5, appear to be engaged in the association with eIF2α, and suggest that full engagement of PKR requires eIF2α to adopt an open conformation.

### *Molecular movements induced by transition between different states of PKR*

To model the collective motions by which PKR transitions between different states, we conducted normal mode analysis of the dominant motion of the KD dimer and the KD dimer-eIF2α complex (Figure 3 and Supplementary Figure S1). These calculations predict that the N-terminal β4-β5 segment of the KD is the most dynamic region before binding with eIF2α. Upon binding of the substrate, eIF2α becomes the most dynamic part of the protein complex and the previously dynamic regions of the KDs are constrained (Figure 3A and B). Although the β4-β5 segment is still the most dynamic part of the KD, its fluctuation drops from 1.5 to less than 0.1 Å. Hence, substrate binding appears to stabilize the PKR dimer. Figure 3B shows the stability changes of the KD dimer alone or in complex with eIF2α in either state ('open' or 'closed'). Contrary to the greater flexibility predicted for isolated eIF2α when in the open state (Figure 1A), the molecule is more dynamic in the closed state when bound to the PKR KD (Figure 3B). Hence, these predictions suggest that the β3-β4 loop on eIF2α must adopt an open conformation in order to form a more stable interaction form with PKR. Additionally, the constraint of the β4-β5 loop of PKR upon binding of eIF2α suggests some association between this element on PKR and the β3-β4 loop on eIF2α. No previous mechanism of kinase activity has invoked an association between the β4-β5 loop of PKR and eIF2α, so we experimentally tested these predictions below.

### *Requirement of the β4-β5 loop of PKR for the control of eIF2α*

To measure the consequence for the β4-β5 loop of PKR to its function we assessed phosphorylation of eIF2α and the resulting control of protein translation by reporter assays and by conducting polysome analysis.

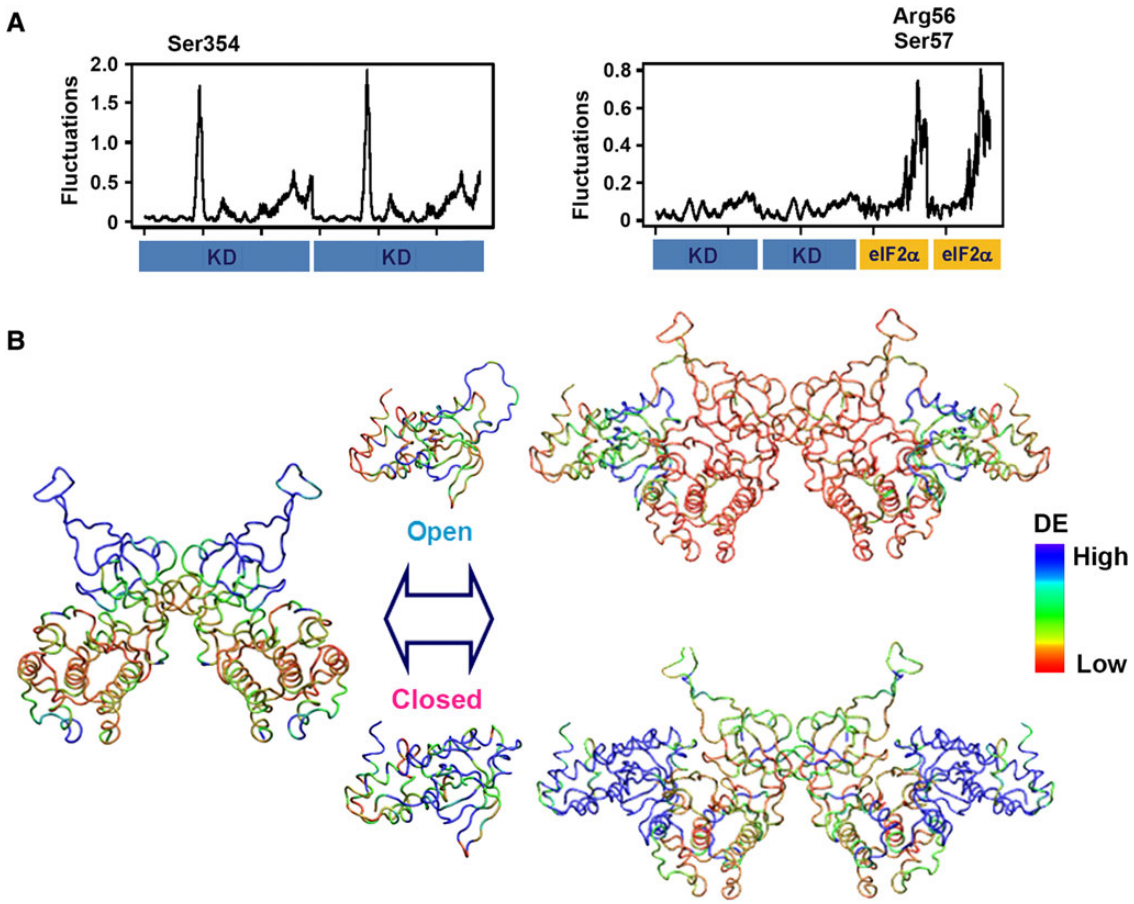


**Figure 3** Molecular movements induced by the association between PKR and eIF2α. (**A**) The theoretical dominant modes of motion of the dimeric KD of PKR alone (left) and upon docking with eIF2α (right). (**B**) Stability changes in the complex between the dimeric KD and eIF2α in either the open or closed conformation. Deformation energy (DE), as analyzed by NMA, throughout the protein complex is depicted with color on an assembled average conformation of the protein backbone. Blue indicates regions above the deformation threshold (more flexible regions), green represents regions that are greater than the deformation threshold, and red corresponds to small deformation energies (more rigid regions). These images show the overall stability of the complex as the averaged deformation changes of the collective dominant modes. The separate dominant modes that account for the majority of the molecule's dynamic movement are shown in Supplementary Figure S1.

Direct phosphorylation of eIF2α was measured using phospho-specific antibodies, after transfecting PKR constructs into modified HEK293 cells (HEK293:shPKR) that express a short hairpin RNA to diminish the expression of endogenous PKR by RNA interference (Figure 4A and B). Appropriately, mutations of the invariant ATP-binding and transfer lysine residue number 296 within the catalytic pocket, or residues demonstrated to perturb formation of the fully active dimer, Arg262, and to affect substrate binding of Thr487 to alanine all diminished eIF2α phosphorylation (Figure 4A) (Katze et al., 1991; Dar et al., 2005). Importantly, residues between the β4-β5 loop of PKR were shown to control eIF2α phosphorylation, with deletion of this loop (construct Δ338–350) as detrimental in this assay as mutation of the residues previously established to be essential for kinase activity (K296R, R262D, and T487A) (Figure 4A).

Phosphorylation of eIF2α increases its affinity for the guanine nucleotide exchange factor eIF2B, thereby preventing exchange of GDP and reformation of the ternary complex that permits succeeding ribosomes to transition along the mRNA. Wild-type (WT) or mutant PKR and PERK constructs were transfected into HEK293:shPKR cells and the effect upon the pattern of ribosomal binding to the mRNA measured. Growth of cells expressing WT PKR greatly increased the accumulation of ribosomes on the mRNA (Figure 5A and E). This is consistent with loading of stalled ribosomes onto the 5′ mRNA. Notably, knocking down the eIF2B2 regulatory subunit of eIF2B, thereby duplicating the effect of eIF2α phosphorylation by alternately limiting the nucleotide exchange factor, replicated the PKR-induced accumulation of ribosomes on the mRNA (Figure 5B and F). This effect of PKR was dependent on kinase activity, demonstrated by expression of the catalytically inactive PKR (K296R) (Figure 5A). Critically, deletion of the β4-β5 segment (Δ338–350) of PKR reduced the high molecular weight fraction of the polysome profile to be equivalent to that of the kinase-dead mutant (Figure 5A). To test the possibility that the β4-β5 loop was affecting kinase activity via modulating an intra-molecular association with the N-terminal RBD of PKR,

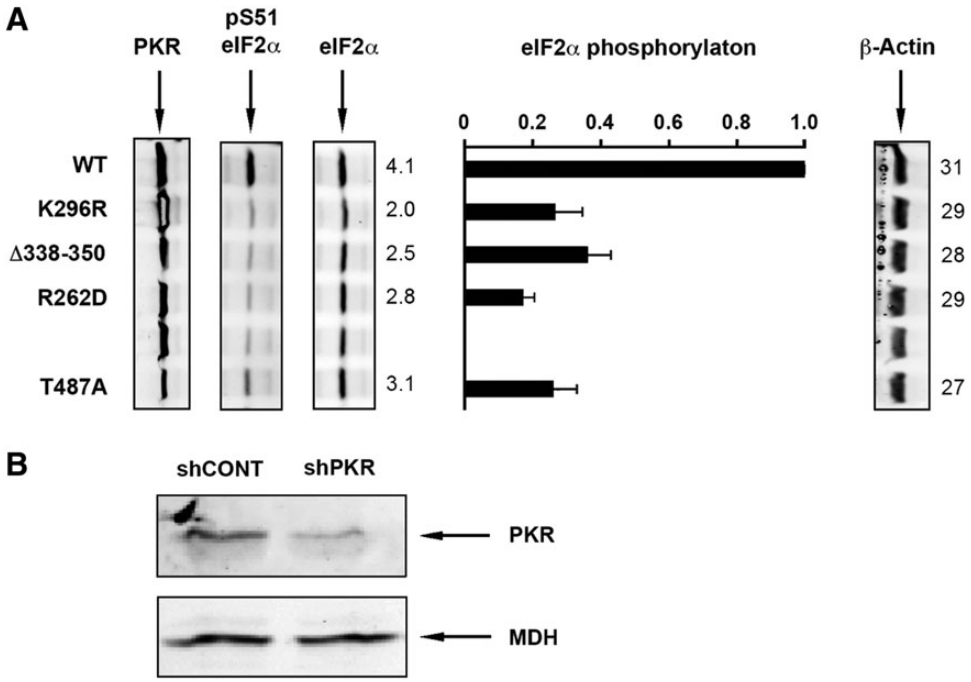


**Figure 4** Measure of the function of the β4-β5 loop of PKR by eIF2α phosphorylation. (**A**) Immunoblot assays for eIF2α phosphorylation from HEK293:shPKR cells transfected with PKR constructs (as labeled). A representative blot for each antigen is shown. The graph shows a quantitation of phosphorylated eIF2α relative to the total levels of eIF2α normalized to the WT PKR treatment for comparison ($n = 4$ for WT, K296R, and Δ338–350 PKR, $n = 3$ for R262D and T487A constructs, error bars show SD). The unlabeled lane involved a protein construct of extraneous activity. The numerals on the right of the blots are a quantification of the protein bands. Expression of the K296R protein is relatively high, which has resulted in overexposure and bleaching of the detected band. Dots evident in the β-actin immunoblot represent a nonspecific signal. (**B**) Immunoblot detection of PKR in HEK293:shPKR cells used in cell-based assays. Endogenous PKR was decreased through stable expression of a short-hairpin RNA that targeted the 3′UTR of *EIF2AK2* (shPKR). Specific targeting of PKR is demonstrated by comparison to a scrambled nontargeting control shRNA (shCONT). The relative expression of PKR is compared with the levels of the metabolic enzyme malate dehydrogenase (MDH).

we assessed the activity of the isolated KD. This demonstrated that the β4-β5 loop regulates the activity of the KD, independent from auto-regulatory mechanisms (Figure 5C and G). Finally, we demonstrated that the equivalent region of the PERK KD also regulated ribosomal activity (Figure 5D and H).

We further assessed eIF2α phosphorylation by measuring protein translation using a fluorescent reporter assay. Expression constructs of the PKR, PERK, and GCN2 KDs were generated as the WT peptide with a point mutation to promote kinase activity (K429R, F927H, and Y838H in PKR, PERK, and GCN2, respectively (Dey et al., 2005a)) and with the β4-β5 insert segment removed (Δ338–350, Δ706–868, and Δ659–782 for PKR, PERK, and GCN2, respectively) (Figure 6A). Firstly, titration of the PKR KD constructs in this reporter assay demonstrated that the β4-β5 loop is not indispensable but that the activity of the truncated kinase (Δ338–350) is severely diminished (Figure 6B). Repetition of the reporter assay with PKR, PERK, and GCN2 demonstrated that the β4-β5 segment is important for translational control of all three kinases (Figure 6C). Hence, the flexible β4-β5 loop within the N-lobe of eIF2α kinases is important for eIF2α phosphorylation, the ensuing regulation of ribosome activity and protein production.

*Residues within the β4-β5 loop of PKR modulate the interaction with eIF2α*

To test if the β4-β5 loop modulates the interaction between PKR and eIF2α under physiological conditions, we employed a bimolecular fluorescence complementation assay (Hu et al., 2002; MacDonald et al., 2006). WT and mutant human PKR constructs were assessed for their capacity to associate with eIF2α by fusing either protein partner to split Venus tags. The impact of specific residues within PKR to the association with eIF2α was quantified as the fluorescent Venus signal, generated by formation of the complete Venus fluorophore upon heterodimerization of the protein partners, normalized to the levels of protein expression, measured by immunofluorescence in HEK293:shPKR cells (Figure 7A–C). Somewhat unexpectedly, this assay showed that kinase-dead protomers (K296R) efficiently associated with eIF2α. Moreover, a mutation in the helix αG, T487A, which ablated phosphorylation of eIF2α (Figure 4A), nevertheless, did not inhibit an association between the proteins (Figure 7A). Hence, it appears that the Thr487 residue is critical only for phosphorylation but not interaction with eIF2α, as had been assumed from yeast growth assays (Dey et al., 2005a). Mutation of a residue previously identified to be essential to formation of the active dimeric kinase,

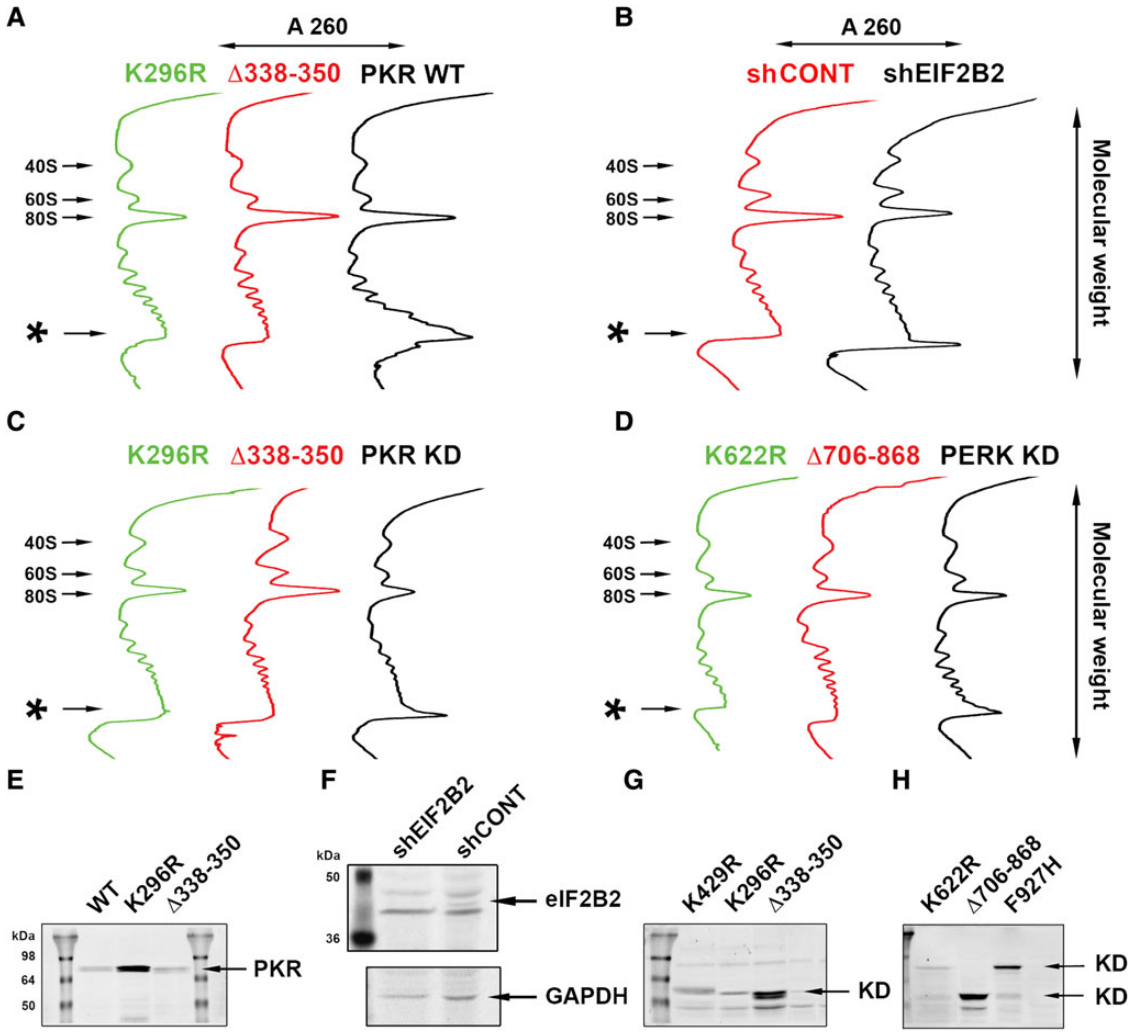


**Figure 5** Measure of the function of the β4-β5 loop of PKR by polysome analysis. (**A**–**D**) The absorbance (260 nm) profile of fractionated whole-cell lysate from: (**A**) HEK293:shPKR cells expressing full-length PKR (WT), this protein with the β4-β5 loop removed (Δ338–350), or an inactivating mutation (K296R); (**B**) HEK293 cells expressing a nontargeting shRNA (shCONT), or targeting eIF2B2 (shEIF2B2); (**C**) HEK293:shPKR cells expressing the PKR KD only with an activating mutation (K429A) alone, and the β4-β5 segment removed (Δ338–350), or with an inactivating mutation (K296R); (**D**) HEK293:shPKR cells expressing the PERK KD with an activating mutation (F927H) alone, and the β4-β5 segment removed (Δ706–868), or with an inactivating mutation (K622R). Absorbance peaks within the profile corresponding to the position of the ribosomal subunits (40S and 60S), assembled monosome (80S) and sequentially increasing polysomes culminating in a high molecular weight fraction (*) are indicated with arrows on the left of the profiles. Polysome assays were repeated a minimum of three times for each kinase construct and a representative profile presented. (**E**–**H**) Western blots detecting the expression of the indicated kinase constructs, or endogenous eIF2B2 in HEK293:shPKR cells. (**E**) Full-length WT, kinase-dead (K296R), and PKR with the β4-β5 loop removed (Δ338–350); (**F**) Endogenous eIF2B2 in HEK293 cells stably expressing shRNAs against the gene (shEIF2B2) or a nontargeting control (shCONT). The concentration of protein in each sample is assessed using an antibody against GAPDH; (**G**) The active (K429R), kinase-dead (K429R+K296R), and truncated (K429R+Δ338–350) KD of PKR; or (**H**) The active (F927H), kinase-dead (F927H+K622R), and truncated (F927H+Δ706–868) KD of PERK, in whole-cell lysates of transiently transfected HEK293:shPKR cells as used in the polysome profiling (**A**–**D**). The kinase constructs were detected using anti-GFP antibodies that recognize the split Venus tags in each construct.

Arg262 (R262D), severely reduced the association with eIF2α (Figure 7A). Putative dynamic residues (Figure 2C) within the ATP-binding loop (Gly276-Gly277) and the β4-β5 loop (Asp338-Asn350) of PKR impaired, without entirely disrupting, the association with eIF2α (Figure 7A).

The fluorescent translational reporter assay was used to probe the functional significance of specific residues within the β4-β5 loop. PKR from species within the primate lineage appear to have undergone a divergent expansion within the β4-β5 insert, so that a broadly conserved motif (DYDPE-S) has been triplicated (Figure 7D). As preliminary mutagenesis suggested there was functional redundancy between these separate motifs, we chose to mutagenize the murine PKR to more simply assess the function of specific residues within the kinase insert region. As for the

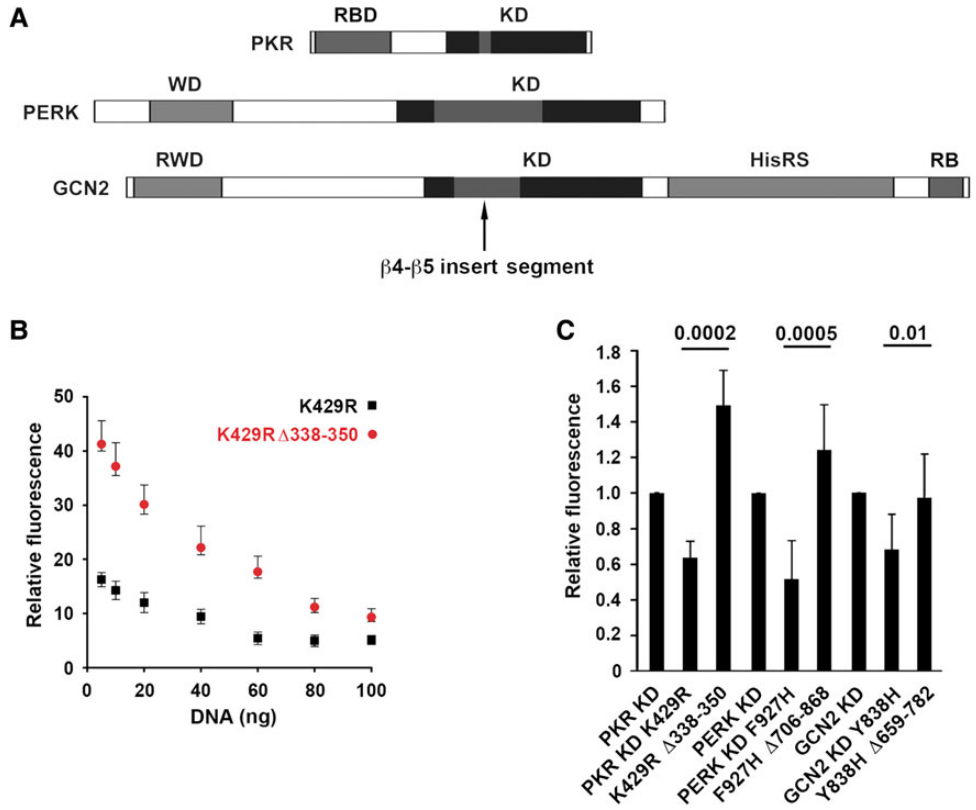


**Figure 6** Measure of the function of the β4-β5 loop of PKR by translational reporter assay. (**A**) A schematic showing the domain structures of three eIF2α kinases: PKR, PERK, and GCN2. The proteins' kinase domains (KD) are shown in black with the β4-β5 insert segment colored gray. The remaining features indicated are the RNA-binding domain (RBD) in PKR, tryptophan-aspartic repeats (WD) in PERK and in GCN2 the histidyl-tRNA synthase-like (HisRS), ribosomal-binding and dimerization (RB) and an analogous protein feature shared between RING finger-containing, WD-repeat-containing and DEAD-like helicase proteins (RWD). (**B**) Protein translation measured as the level of fluorescence produced in HEK293:shPKR cells cotransfected with an RFP reporter and increasing amounts of the active (K429R), or truncated (K429R+Δ338−350) KD of PKR. Data points show the sample means and variance of six replicates of a representative experiment from repeated independent experiments. Statistical significance was measured by linear regression of the intensity of RFP with the PKR constructs and their concentration as covariates ($P < 0.0001$). (**C**) Protein translation measured as RFP in HEK293:shPKR cells cotransfected with various KD constructs of PKR (as labeled), PERK, or GCN2. Fluorescence was normalized to that of the WT KD for each peptide. Statistical significance was measured by *t*-test with four, six, and ten independent experimental replicates for PKR, PERK, and GCN2, respectively.

human kinase, deletion of the murine PKR β4-β5 loop (residues Glu310-Ser317) reduced translational control (Figure 7E). Mutation of residues that were broadly conserved between different species, including Asp306, Tyr307, Asp308, Glu310, Ser312, Ser314, Ser317, or Arg318 to alanine, all affected kinase function (Figure 7E). The relative activity of the different mutant proteins shows that Glu306 had the most significant effect. This residue is at the C-terminus of the β4 element, so it cannot be ruled out that this mutation has altered the structure of the KD. More modest effect on kinase activity is apportioned between the remaining residues. As separate mutations within the β4-β5 loop of murine PKR had an effect on protein function it suggests the effect of this insert segment is not regulated by nonspecific backbone interactions of the amino acids.

## Discussion

Many of the growing number of experimentally determined protein structures capture proteins in low energy, inactive states. This, combined with the requirement to remove dynamic residues to enable protein crystallization and limited measures of protein dynamics, restricts our precise understanding of enzyme activity. Here we have taken advantage of a highly informative static structure deduced for the active, dimeric PKR in association with its substrate eIF2α to generate coarse-grained molecular models of the protein complex. Consistent with an emerging scenario for dynamics carrying allosteric free energy, our analyses predict a transferral of dynamic strength between PKR protomers to the bound substrate that leads to rigidification of PKR as it complexes with eIF2α. Predicted dynamism from these simulations shows that many of the regions that are absent from the current high-resolution structures of eIF2α kinases are dynamic hot spots. Experimental testing of one of these putative dynamic regions demonstrates that residues within the β4-β5 loop control protein function.

Our analysis predicts that the β3-β4 loop of eIF2α adopts two orientations with significant bearing on its competence as a

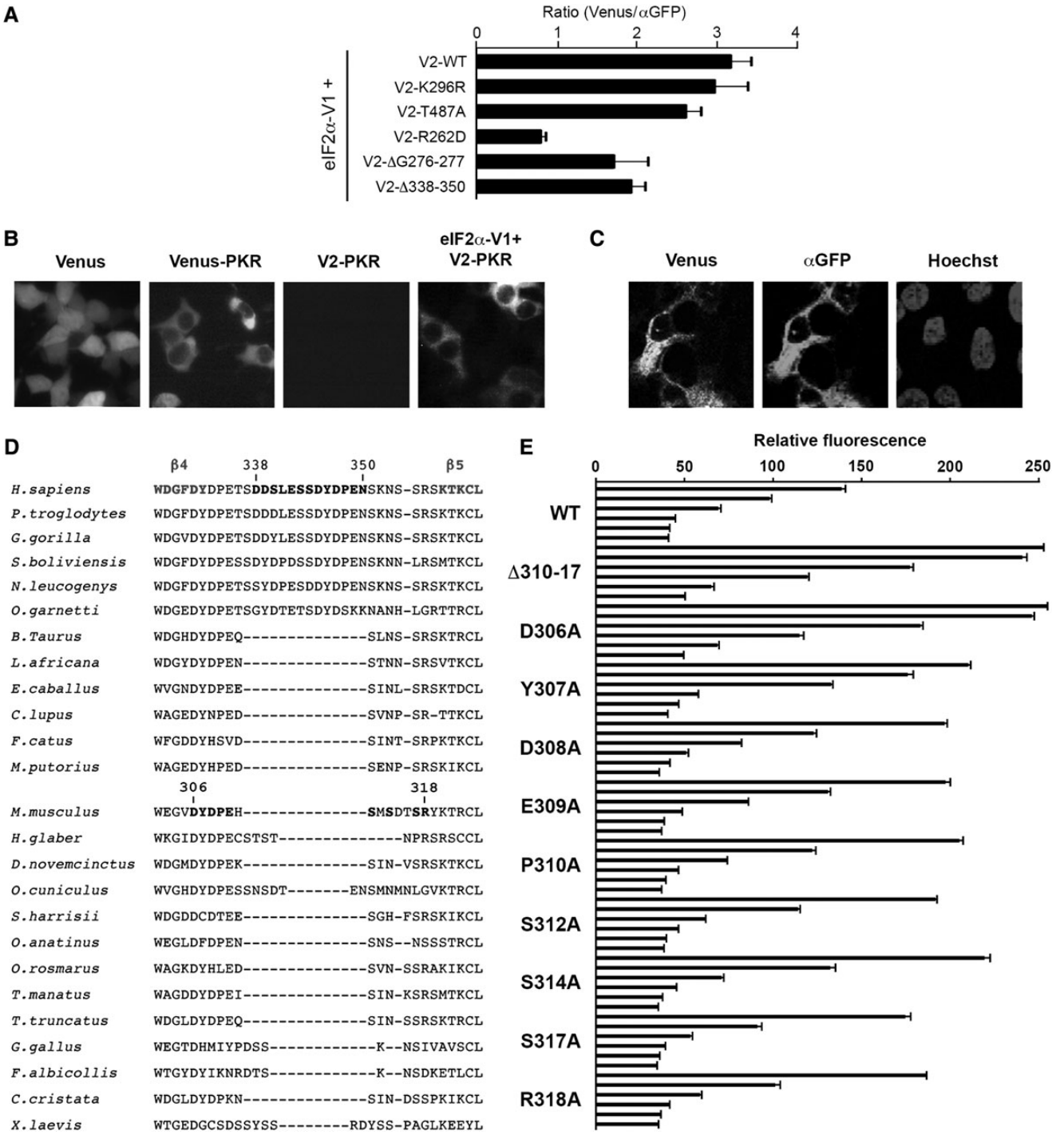


**Figure 7** Functional interrogation of residues within the β4-β5 loop. (**A**–**C**) Quantitation of protein–protein interactions measured as the levels of fluorescence in HEK293:shPKR cells transfected with split Venus fused to eIF2α and PKR constructs. (**A**) The effect of residues in PKR (as labeled) on the protein's interaction with eIF2α. (**B**) Micrographs showing fluorescence in HEK293:shPKR cells transfected with plasmids expressing; Venus alone, Venus tagged to PKR localized in the cell cytoplasm, PKR tagged with the C-terminal half (V2) of a split Venus, and this construct co-expressed with eIF2α tagged with the reciprocal N-terminal (V1) part of a split Venus. (**C**) Micrographs of HEK293:shPKR cells co-expressing V2-PKR and eIF2α-V1 showing the protein association as Venus fluorescence (left), detection of the V2 split protein by immunofluorescence with primary anti-GFP and secondary Alexa647 secondary antibodies (in center) and cell nuclei detected with Hoechst dye (right). (**D**) An alignment of residues within the β4-β5 segment of PKR from diverse species produced using T-Coffee (Notredame et al., 2000). Residues marked in bold indicate the residues mutated in the human, or mouse PKR. Residues colored blue indicate residues constituting part of the β4 and β5 elements within the kinase N-lobe. (**E**) Assay of the functional effect of truncating (Δ310–17), or mutating residues (as indicated) within the β4-β5 segment of murine PKR, measured as inhibition of an RFP translational reporter with increasing concentrations of each construct (0.625, 1.25, 2.5, 5, 10, and 20 ng/well). Data points show the sample means and variance of three replicates of a representative experiment from repeated independent experiments.

substrate. The predicted flexibility of this loop is consistent with the observed disorder of this segment in the PKR–eIF2α crystal structure, as well as by chemical shift measures calculated by NMR (Dar et al., 2005; Dey et al., 2011). Dar et al. (2005), describing the flexibility of this segment, demonstrated that mutation of residues preceding the loop region (most particularly residue Leu47) rescued activity of a mutant PKR, T487A, which had previously been demonstrated to impair phosphorylation of eIF2α. This led to speculation that this mutation either disrupted a hydrophobic network that restricts the position of Ser51 or altered linkage between eIF2α and the kinase-docking region, which has been delineated as the helix αG in the C-lobe of the KD. Our analysis supports the former explanation. Moreover, we propose that residues between β4-β5 within the N-lobe of PKR modify the attitude of this flexible loop on eIF2α. This contrasts with the current dogma that substrate interactions are limited to the C-lobe of the kinase domain. Persuasively, we observed that despite protomers being autophosphorylated and catalytically active (Dar et al., 2005; Dey et al., 2005b), a truncated PKR mutant lacking the β4-β5 loop has reduced capacity to phosphorylate eIF2α, and thus does not effectively control protein translation.

Although ignored in the literature, support for an interaction between segments of eIF2α and the N-lobe of PKR comes from a study that identified substrate contact residues through analysis of amino acid replacement, driven by selective pressure from the poxvirus K3L inhibitor of PKR (Elde et al., 2009). K3L is considered a molecular mimic of eIF2α (Dar and Sicheri, 2002). Elde et al. (2009) demonstrated that residues under positive selection to resist this viral mimicry occurred not only on the C-lobe of PKR (at residues Gln376, Lys380, Phe489, Ser492, and Thr496), but also on the N-lobe, within the β4-β5 loop (at residues Thr336, Asp338, Ser344, and Ser351) (Elde et al., 2009). Concordant with this, it was demonstrated that mutation of a residue (Val52) located within the helical insert of K3L, which does not contact the established substrate-binding structures (the αG helix) of PKR within the C-lobe of the KD, but that would be predicted to contact the β4-β5 loop of PKR, diminished inhibition of PKR (Dar and Sicheri, 2002). The structural similarity and inherent mode of action of K3L, to compete with eIF2α for binding to PKR, suggest that the segment between β4 and β5 would also contact eIF2α.

A previous study reported that deletion of a larger region of PKR (residues Phe330 to Ser355) ablated kinase activity (Craig et al., 1996). To try to confirm that the loss of activity was not due to disruption of the protein structure by this truncation, a shorter region was removed (Phe330-Thr336) and several point mutations (Y323F, S337A, and S355A) were generated. The residues in this shorter truncation are outside of that demonstrated here and still encompass part of the β4 element. Therefore, destabilization of the kinase structure cannot be excluded. Our mutagenesis of residues at the carboxyl terminus of the β4 element of the murine PKR also perturbed enzyme activity. Of the point mutations tested, the residue Ser355 was identified as being crucial to kinase activity as measured by repression of yeast growth (Tzamarias and Thireos, 1988). Again, this residue is outside of the region identified in this study. Moreover, we were unable to corroborate a function for this residue by fluorescent reporter assay in human cells (Supplementary Figure S2). The location of the Ser355 residue is distant from eIF2α in the protein complex, so does not accord with the speculated interaction with the β3-β4 loop of eIF2α.

We demonstrate here that the β4-β5 segment fulfills the same role in other eIF2α kinases. Interestingly, this segment is enlarged in the eIF2α kinases relative to many other protein kinases. We posit that this relates to a transferral of substrate recognition, solely from the C-lobe, to include both lobes of the eIF2α kinases. The apparent increased importance of the β4-β5 segment in the eIF2α kinases is consistent with the suggestion of a requirement for more stringent control of substrate phosphorylation, to enable translation in the face of multiple eIF2α kinases that respond to diverse stimuli (Dey et al., 2011). However, rather than the speculation that this specificity was solely dictated by the position of the helix αG in the C-lobe, which is atypical for the eIF2α kinases (Dar et al., 2005; Padyana et al., 2005; Cui et al., 2011), we propose that increased specificity in this kinase family is also afforded through additional contacts with residues in the N-lobe of the KD.

Analogous to our finding for the eIF2α kinases, residues within the β4-β5 segment of the transforming growth factor-β (TGF-β) type-I receptors have also been shown to control substrate phosphorylation. Residues within this segment (termed the L45 loop) of the kinase domain contact residues within the L3 loop of the different SMAD substrate proteins to regulate specific transcriptional responses (Feng and Derynck, 1997; Chen et al., 1998). Still other instances of this mechanism appear to have been identified (Kazlauskas and Cooper, 1989; Carlberg et al., 1991). The β4-β5 segment of the TGF-β receptor family, also, encodes additional residues from the majority of protein kinases. Approximately 60 kinases have an extended β4-β5 segment (Hanks and Quinn, 1991) (http://kinase.com/human/kinome/phylogeny.html). If merely the length of this segment is predictive of contacts to the protein substrates, then the mode of action identified for the eIF2α and TGF-β receptor kinases may comprise a recurrent mechanism of kinase action. In most, if not all, crystallographic protein kinase structures this segment has been removed. Hence, the significance of this region for the function of protein kinases has been largely overlooked.

In summary, we generate a theoretical full-length structure of eIF2α and the KD of PKR that is tested for its ability to replicate previously observed protein states derived from modified peptides. Functional interrogation using mutagenesis coupled with analysis of the state and activity of the proteins, demonstrated that dynamic residues predicted within both molecules, which are removed or unresolved in current experimentally derived structures, are critical for enzyme activity. Importantly, we demonstrated that the β4-β5 loop within the N-lobe of the KD is important for substrate phosphorylation and posit that this is required to correctly position the serine phosphor-residue within the flexible β3-β4 loop of eIF2α. Figure 8 shows a model that reinterprets the current mechanism of action of PKR to account for the critical role of flexible loops in the N-lobe outside of the canonical substrate-binding region in the C-lobe of the kinase domain and encompassing the serine phosphor-residue in the substrate.

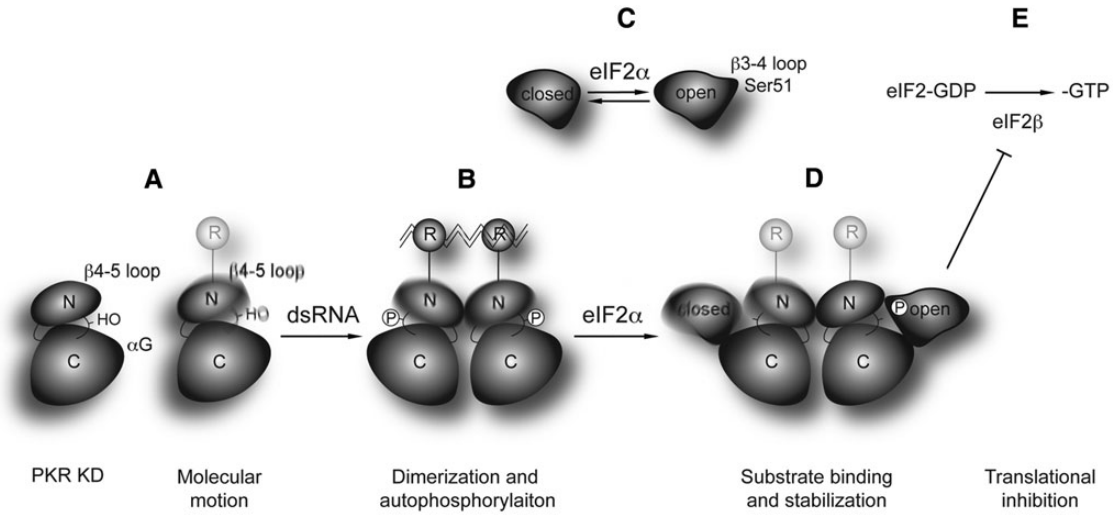


**Figure 8** A revised model of the catalytic steps of PKR activation and function. (**A**) A schematic indicating the β4-β5 loop within the N-lobe (N) and the substrate-binding αG helix within the C-lobe (C) of the PKR KD. The inactive PKR monomer has dynamic motion (depicted by blurring of elements in the right graphic), particularly within the N-lobe at the β4-β5 loop. (**B**) The inactive monomer is activated by binding of RNA (zigzag line) at the protein's RBD (R), which initiates dimerization and stimulates autophosphorylation within the kinase activation loop (P). (**C** and **D**) Active, dimeric PKR associates with eIF2α in one of two conformations (with regard to the orientation of the β3-β4 loop as depicted in **C**) that have different fitness as substrates. Stabilization of the β3-β4 loop of eIF2α in the open conformation diminishes the dynamic motion of the entire protein complex (contrasted on the left and right of the complex in **D**), thereby enabling phosphorylation of the serine residue number 51 of eIF2α that is embodied within the β3-β4 loop. (**E**) Phosphorylated eIF2α inhibits protein translation by sequestering the guanine nucleotide exchange factor eIF2B.

## Materials and methods

*Structures and molecular modeling of PKR–eIF2α*

The theoretical structures of PKR and KD-eIF2α were obtained by using the atomic coordinates of PDB:2A1A and PDB:1QU6, for the KD-eIF2α and RBD as the initial input structures. The missing segments and residues from the KD (residues 338–354 and 542–551), eIF2α (residues 49–60), and RBD (residues 1–9 and 169–254) were restored by bioinformatics and structural modeling methods. A coarse-grained dynamics and normal mode analysis algorithm based on an elastic network model of protein was then applied. The theoretical temperature factors (B-factors) agree well with the backbone dynamics derived from NMR measurements and X-ray diffractions.

*Modeling, simulation, and visualizations*

The modeled structures for different conformational states of PKR were first relaxed by molecular mechanics (MM) minimization before the NMA/GNM and COREX computations. The MM minimization was performed using ~2000 steps by NAMD (Kalé et al., 1999) with threshold energy less than $10^{-4}$ kcal $mol^{-1}$ $Å^{-1}$. The dynamics minimization and normal modes analysis were carried out on a Linux cluster of 195 × 4 Quad-core Intel CPUs. Typically it takes only a few CPU minutes (<5 min) to accomplish an NMA/GNM calculation of PKR (~1100 residues for dimer) or MM computing (in parallel mode). Structural modeling, analysis and graphics visualization were processed by the Virtual Molecular Dynamics (VMD) package (Humphrey et al., 1996).

*Dynamic fluctuations and correlations in PKR*

Dynamic correlations in proteins can be interpreted by the dynamics of cross-correlations among residue fluctuations when the protein undergoes conformational changes (Liu et al., 2006, 2008). As the covariance matrix calculates the correlated fluctuations of atoms throughout the protein, to determine coupling between intra- and inter-domain changes, we define a difference correlation matrix of motions between two discrete conformations of protein, e.g. upon ligand binding, as (Liu et al., 2008),

$$C_{AB} = \frac{C_{ij}^{A} - C_{ij}^{B}}{2} = \frac{\langle \Delta \boldsymbol{r}_i \cdot \Delta \boldsymbol{r}_j \rangle^{A} - \langle \Delta \boldsymbol{r}_i \cdot \Delta \boldsymbol{r}_j \rangle^{B}}{2} \quad (1)$$

where *A* and *B* refer to two dynamically distinguished conformations. For example, they may refer to the 'open' and 'closed' states, and transient conformers between them. The diagonalized and normalized $C_{AB}$ should have values varying from −1, 0 to +1, showing the strongly correlated, noncorrelated, and strongly anticorrelated motions between conformations of *A* and *B*. The term $\langle \Delta r_i \cdot \Delta r_j \rangle$ refers to the variance-covariance matrix of the atomic fluctuations between atom *i* and atom *j*. This matrix can be derived from dynamics data from either experimental measurements or molecular simulations. However, both experimental methods and molecular dynamics simulations currently have great difficulty in handling large biomolecules over long timescales. Here, an alternative approach is used for an accurate, and computationally fast, determination of $\langle \Delta r_i \cdot \Delta r_j \rangle$. Using the

dynamics algorithm of an improved Gaussian network model (GNM) (Bahar et al., 1997), the atomic details of a protein can be coarse-grained by a Gaussian elastic network of its backbone $C^{\alpha}$ atoms. Mean-square fluctuations of residues, or the cross-correlations, can then be determined via (Tobi and Bahar, 2005),

$$\langle \Delta \boldsymbol{r}_i \cdot \Delta \boldsymbol{r}_j \rangle = \frac{3k_B T}{\gamma} [\Gamma^{-1}]_{ij} \tag{2}$$

where $\gamma$ is a theoretical parameter mimicking the strength of the harmonic potential of the elastic network of $C^{\alpha}$ atoms. $[\Gamma^{-1}]_{ij}$ is the $ij$th element of the inverse Kirchhoff matrix $\Gamma$, a symmetric matrix also known as the valency adjacency matrix in graph topology theory. In the GNM approximation, the elements of $\Gamma$ are given by (Bahar et al., 1997),

$$\Gamma_{ij} = \begin{cases} -1 & \text{if} \quad i \neq j \quad \text{and} \quad r_{ij} \leq r_C \\ 0, & \text{if} \quad i \neq j \quad \text{and} \quad r_{ij} \leq r_C \\ -\sum_{i \neq j} \Gamma_{ij} & \text{if} \quad i = j \quad \text{and} \end{cases} \tag{3}$$

The summation for evaluating $\Gamma_{ij}$ is performed over all off-diagonal elements on the $i$th residue at a cutoff distance of $r_C$, which defines the range of interactions between residues. The mean-square fluctuations of $C^{\alpha}$ atoms from Equation (2) also lead to theoretical temperature B-factor values, i.e. $B_i = 8\pi^2 \cdot \langle \Delta r_i \cdot \Delta r_i \rangle / 3$, which compare well with X-ray crystallography measurements and other methods (Bahar et al., 1997).

*Normal mode analysis using elastic network model*

Normal mode analysis (NMA) provides an approximation of protein motions by expanding the motion into a superposition of different normal modes of vibrations, where each normal mode is characterized by a frequency of vibration of overdamped dynamics. Low frequency NMA modes using elastic network models have been applied widely to globular proteins (Delarue and Dumas, 2004; Ma, 2005) to describe their collective dynamics, dynamic domains, hinge-bending motion, and other functionally important motions. As proteins perform most biological functions dynamically starting near the native states, NMA using elastic network model of proteins is based on a harmonic perturbation approximation of the potential energy function around a global minimum conformational state. Therefore, NMA captures the intrinsic modes of motions encoded in the protein structures. Conformational transitions in proteins, such as open/closed conformers upon ligand binding or oligomerization due to protein–protein interaction, can be well captured via normal mode analysis.

NMA can discriminate conformation changes between large-scale, long-range amplitude motions (via low-frequency modes) and confined, local motions (via high-frequency modes). The relative importance of normal modes in a particular conformational change is evaluated in terms of collectivity and overlap coefficients (Delarue and Dumas, 2004). Collectivity measures the collective degree of protein motion in a certain mode, i.e. the number of residues significantly involved in that mode. In this work, NMA was performed mainly with the GNM algorithm (Bahar et al., 1997), where the protein structure details were coarse-grained by a Gaussian elastic network of the backbone $C^{\alpha}$ atoms. Fluctuation and flexibility (interpreted as the residue temperature B-factor) were derived by Equation (2). Dynamic correlations in conformational transitions were determined by Equation (1). More detailed NMA results of PKR dimerization and interaction with eIF2α are provided in Supplementary material.

*Dynamic stability analysis*

To determine dynamic stabilities of the PKR–eIF2α complex, a COREX/BEST algorithm (Vertrees et al., 2005) can also be employed where the fluctuations for different conformational states, e.g. the inactive and active states, are sampled by statistical thermodynamics rather than structural states. COREX/BEST produces a stability constant at each residue as thermodynamic metric, wherein each of the static structural properties is weighted according to its energetic impact (e.g. surface area, polarity, and packing are implicitly considered). The dynamic nature of stability means that residues with high stability constants will be less flexible and will fold in the majority of highly probable states. On the other hand, residues with low stability constants will be more flexible and less likely to be folded in many of the highly probable states.

*Bimolecular complementation assays*

Bimolecular complementation assays were performed as previously described (Hu et al., 2002; MacDonald et al., 2006) in HEK293:shPKR cultured in DMEM supplemented with 10% fetal bovine serum under puromycin (10 μg/ml) selection, at 37°C in a 5% $CO_2$ humidified incubator. Levels of Venus fluorescence were normalized to protein expression, measured by immune analysis (Figure 7C). Cells ($0.5 \times 10^5$/well) plated onto confocal glass coverslips, in a 24-well plate (BD Falcon), were fixed in 10% formalin for 5 min, before rinsing and permeabilizing in 0.1% Triton-X 100 in PBS for 5 min prior to treatment with CAS-block (Invitrogen) for 30 min. Either half of the split Venus protein was detected with the primary monoclonal anti-GFP antibodies, 7.1 and 13.1 (Roche), or B34 (Covance), followed by Alexa647 or 594 labeled secondary antibodies, and imaged on the Leica SP5 multichannel under eYFP conditions or on a Nikon C1 confocal (GFP settings).

*Immunoanalysis*

Western blot analysis was conducted by transferring whole-cell lysates to Immobilon-FL, probing with primary antibodies followed by Alexa 680 nm or IRdye800 nm secondary antibodies, then visualizing by Licor-Odyssey (Biosciences). Primary antibodies consisted of the rabbit polyclonal eIF2α[pS52]PAb, eIF2αPAb (Invitrogen), rabbit monoclonal antibody YE350 (Abcam), rabbit polyclonal EIF2B2 (Abcam), and mouse monoclonal GAPDH (Abcam). Western blots were quantified with NIH Image J using sum intensity of the OD profile plots, with background correction calculated per lane.

*Assays of protein translation*

A fluorescent reporter was generated that expressed monomeric red fluorescent protein (RFP) under control of an RNA polymerase III U6 promoter enhanced with the RNA polymerase II cytomegalovirus promoter in a pBluescript (Stratagene) backbone plasmid.

The level of RFP was measured using a Typhoon Trio (GE Healthcare). The isolated kinase domains of PKR, PERK, and GCN2 were constructed (in the pcDNA3.1) as described previously (Dey et al., 2005a; Padyana et al., 2005; Cui et al., 2011). The various point mutations and truncations were introduced by PCR.

Ribosomal analysis was conducted with HEK293 expressing shRNAs (SIGMA) against PKR, eIF2B2, or a nontargeting shRNA. One μg of each kinase construct was transfected into $2 \times 10^6$ cells in a 6 cm dish, then passaged after 24 h into three 10 cm dishes and grown for a further 24 h until reaching 50% confluence. The cells were treated with 100 μM of cycloheximide (SIGMA) for 10 min at 37°C, rinsed and suspended in ice-cold PBS with 100 μM of cycloheximide by scraping the cells from the plate. The cell suspension was pelleted at 4°C, resuspended in ice-cold cell lysis buffer (10 mM HEPES-KOH, pH 7.9, 2.5 mM $MgCl_2$, 100 mM KCl, 1 mM DTT, 0.1% Nonidet P-40, 100 units/ml RNase inhibitor and 100 μg/ml cycloheximide), homogenized by passing through a 25-gauge syringe needle, and centrifuged at 6000 rpm for 15 min to remove cell debris. The cleared cell extract (5–10 $A_{260}$ units) was fractionated by centrifugation in a Beckman optimal L-90K ultra-centrifuge at 16500 rpm for 20.5 h using a SW41 rotor through a discontinuous 10%–50% sucrose gradient (prepared in 10 mM HEPES-KOH pH 7.9, 2.5 mM $MgCl_2$, 100 mM KCl, and 1 mM DTT) that had been frozen then thawed. The fractionated sample was displaced from the centrifugation tube by pumping a 60% sucrose solution into the bottom of the tube and the ribosomal loading on mRNA assessed by measuring absorbance at 260 nm using a Brandel BR-18b-5 fractionator system.

*Statistical analysis*

The statistical applications within Microsoft Excel, or the program R-2.14.0 (http://R-project.org) was used to analyze the data.

## Supplementary material

Supplementary material is available at *Journal of Molecular Cell Biology* online.

## Acknowledgements

We thank Drs Stephen Michnick and Jean-François Paradis (University of Montreal) for their split Venus plasmids, Dr Steve Bouralexis for access to the Typhoon Trio scanner, Dr Matthew Belousoff for his help with polysome analysis, Dr Di Wu for statistical analysis, Dr Dakang Xu for comments, and Dr Frances Cribbin for her editorial assistance.

## Funding

This work is supported by an Australian Research Council (http://www.arc.gov.au) Discovery Project Grant DP110102641, an Australian National Health and Medical Research Council (http://www.nhmrc.gov.au) Project Grant APP1043398, the Victorian Government (http://www.vic.gov.au) Operational Infrastructure Support Program, and the CSIRO (http://www.csiro.au) Australian Biotech Growth Partnership and Advanced Materials TCP. Generous allocations of computing resources from the National Computational Infrastructure of Australia (http://nci.org.au) are also acknowledged. The funders had no role in study design, data collection and analysis, decision to publish, or preparation of the manuscript.

**Conflict of interest:** none declared.

## References

Bahar, I., Atilgan, A.R., and Erman, B. (1997). Direct evaluation of thermal fluctuations in proteins using a single-parameter harmonic potential. Fold. Des. *2*, 173–181.

Carlberg, K., Tapley, P., Haystead, C., et al. (1991). The role of kinase activity and the kinase insert region in ligand-induced internalization and degradation of the c-fms protein. EMBO J. *10*, 877–883.

Chen, Y.G., Hata, A., Lo, R.S., et al. (1998). Determinants of specificity in TGF-beta signal transduction. Genes Dev. *12*, 2144–2152.

Craig, A.W., Cosentino, G.P., Donze, O., et al. (1996). The kinase insert domain of interferon-induced protein kinase PKR is required for activity but not for interaction with the pseudosubstrate K3L. J. Biol. Chem. *271*, 24526–24533.

Cui, W., Li, J., Ron, D., et al. (2011). The structure of the PERK kinase domain suggests the mechanism for its activation. Acta Crystallogr. D Biol. Crystallogr. *67*, 423–428.

Dar, A.C., and Sicheri, F. (2002). X-ray crystal structure and functional analysis of vaccinia virus K3L reveals molecular determinants for PKR subversion and substrate recognition. Mol. Cell *10*, 295–305.

Dar, A.C., Dever, T.E., and Sicheri, F. (2005). Higher-order substrate recognition of eIF2alpha by the RNA-dependent protein kinase PKR. Cell *122*, 887–900.

Delarue, M., and Dumas, P. (2004). On the use of low-frequency normal modes to enforce collective movements in refining macromolecular structural models. Proc. Natl Acad. Sci. USA *101*, 6957–6962.

Dey, M., Cao, C., Dar, A.C., et al. (2005a). Mechanistic link between PKR dimerization, autophosphorylation, and eIF2alpha substrate recognition. Cell *122*, 901–913.

Dey, M., Trieselmann, B., Locke, E.G., et al. (2005b). PKR and GCN2 kinases and guanine nucleotide exchange factor eukaryotic translation initiation factor 2B (eIF2B) recognize overlapping surfaces on eIF2alpha. Mol. Cell. Biol. *25*, 3063–3075.

Dey, M., Velyvis, A., Li, J.J., et al. (2011). Requirement for kinase-induced conformational change in eukaryotic initiation factor 2alpha (eIF2alpha) restricts phosphorylation of Ser51. Proc. Natl Acad. Sci. USA *108*, 4316–4321.

Elde, N.C., Child, S.J., Geballe, A.P., et al. (2009). Protein kinase R reveals an evolutionary model for defeating viral mimicry. Nature *457*, 485–489.

Feng, X.H., and Derynck, R. (1997). A kinase subdomain of transforming growth factor-beta (TGF-beta) type I receptor determines the TGF-beta intracellular signaling specificity. EMBO J. *16*, 3912–3923.

Hanks, S.K., and Quinn, A.M. (1991). Protein kinase catalytic domain sequence database: identification of conserved features of primary structure and classification of family members. Methods Enzymol. *200*, 38–62.

Hu, C.D., Chinenov, Y., and Kerppola, T.K. (2002). Visualization of interactions among bZIP and Rel family proteins in living cells using bimolecular fluorescence complementation. Mol. Cell *9*, 789–798.

Humphrey, W., Dalke, A., and Schulten, K. (1996). VMD—visual molecular dynamics. J. Mol. Graph. Model. *14*, 33–38.

Kalé, L., Skeel, R., Bhandarkar, M., et al. (1999). NAMD2: greater scalability for parallel molecular dynamics. J. Comput. Phys. *151*, 283–312.

Katze, M.G., Wambach, M., Wong, M.L., et al. (1991). Functional expression and RNA binding analysis of the interferon-induced, double-stranded RNA-activated, 68,000-Mr protein kinase in a cell-free system. Mol. Cell. Biol. *11*, 5497–5505.

Kazlauskas, A., and Cooper, J.A. (1989). Autophosphorylation of the PDGF receptor in the kinase insert region regulates interactions with cell proteins. Cell *58*, 1121–1133.

Liu, M.S., Todd, B.D., and Sadus, R.J. (2006). Dynamic and coordinating domain motions in the active subunits of the F1-ATPase molecular motor. Biochim. Biophys. Acta *1764*, 1553–1560.

Liu, M.S., Todd, B.D., Yao, S., et al. (2008). Coarse-grained dynamics of the receiver domain of NtrC: fluctuations, correlations and implications for allosteric cooperativity. Proteins *73*, 218–227.

Ma, J. (2005). Usefulness and limitations of normal mode analysis in modeling dynamics of biomolecular complexes. Structure *13*, 373–380.

MacDonald, M.L., Lamerdin, J., Owens, S., et al. (2006). Identifying off-target effects and hidden phenotypes of drugs in human cells. Nat. Chem. Biol. *2*, 329–337.

Notredame, C., Higgins, D.G., and Heringa, J. (2000). T-Coffee: a novel method for fast and accurate multiple sequence alignment. J. Mol. Biol. *302*, 205–217.

Padyana, A.K., Qiu, H., Roll-Mecak, A., et al. (2005). Structural basis for autoinhibition and mutational activation of eukaryotic initiation factor 2alpha protein kinase GCN2. J. Biol. Chem. *280*, 29289–29299.

Sadler, A.J., and Williams, B.R.G. (2007). Structure and function of the protein kinase R. Curr. Top. Microbiol. Immunol. *316*, 253–292.

Tobi, D., and Bahar, I. (2005). Structural changes involved in protein binding correlate with intrinsic motions of proteins in the unbound state. Proc. Natl Acad. Sci. USA *102*, 18908–18913.

Tzamarias, D., and Thireos, G. (1988). Evidence that the GCN2 protein kinase regulates reinitiation by yeast ribosomes. EMBO J. *7*, 3547–3551.

VanOudenhove, J., Anderson, E., Krueger, S., et al. (2009). Analysis of PKR structure by small-angle scattering. J. Mol. Biol. *387*, 910–920.

Vertrees, J., Barritt, P., Whitten, S., et al. (2005). COREX/BEST server: a web browser-based program that calculates regional stability variations within protein structures. Bioinformatics *21*, 3318–3319.